

# DMS: Diffusion-Based Multi-Baseline Stereo Generation for Improving Self-Supervised Depth Estimation

Zihua Liu<sup>1</sup> Yizhou Li<sup>2</sup> Songyan Zhang<sup>3</sup> Masatoshi Okutomi<sup>1</sup>

<sup>1</sup>Institute of Science Tokyo, Japan

<sup>2</sup>Sony Semiconductor Solutions Group, Japan

<sup>3</sup>Nanyang Technological University, Singapore

{zliu<sup>1</sup>, yli<sup>2</sup>, mxo<sup>1</sup>}@ok.sc.e.titech.ac.jp, spyderzsy<sup>3</sup>@gmail.com

## Abstract

While supervised stereo matching and monocular depth estimation have advanced significantly with learning-based algorithms, self-supervised methods using stereo images as supervision signals have received relatively less focus and require further investigation. A primary challenge arises from ambiguity introduced during photometric reconstruction, particularly due to missing corresponding pixels in ill-posed regions of the target view, such as occlusions and out-of-frame areas. To address this and establish explicit photometric correspondences, we propose **DMS**, a model-agnostic approach that utilizes geometric priors from diffusion models to synthesize novel views along the epipolar direction, guided by directional prompts. Specifically, we finetune a Stable Diffusion model to simulate perspectives at key positions: left-left view shifted from the left camera, right-right view shifted from the right camera, along with an additional novel view between the left and right camera. These synthesized views supplement occluded pixels, enabling explicit photometric reconstruction. Our proposed DMS is a cost-free, ‘plug-and-play’ method that seamlessly enhances self-supervised stereo matching and monocular depth estimation, and relies solely on unlabeled stereo image pairs for both training and synthesizing. Extensive experiments demonstrate the effectiveness of our approach, with up to **35%** outlier reduction and state-of-the-art performance across multiple benchmark datasets. The code is available at <https://github.com/Magicboomliu/DMS>.

## 1. Introduction

Depth estimation remains a critical task in computer vision with applications spanning autonomous driving[83], robotic navigation[49], and augmented reality[61]. Although supervised stereo matching [8, 27, 45, 46, 80, 91, 93] and

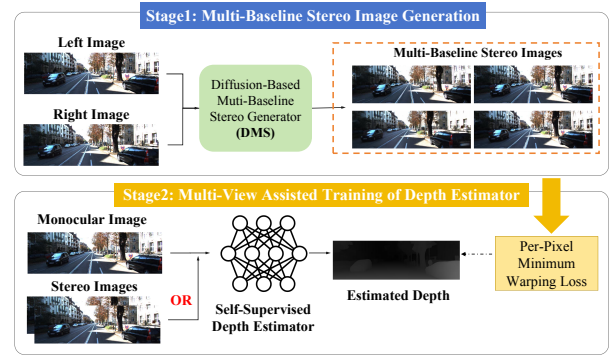


Figure 1. Overview of the proposed Diffusion-based Multi-Baseline Stereo Generation (DMS) pipeline. Given the left and right input views, DMS generates additional multi-baseline views for the scene, which are then used to enhance self-supervised depth estimation through our Per-Pixel Minimum Warping Loss.

monocular depth estimation [4, 5, 84–86] have made substantial progress with deep learning, self-supervised methods using stereo images as supervision signals have become an appealing alternative, circumventing the costly need for labeled depth data. However, self-supervised methods face significant challenges, especially in occluded and out-of-frame regions where pixel correspondences are missed.

Recent methods have attempted to mitigate the issues in these ill-posed regions by inferring or propagating context information [17, 36, 71, 82, 89, 95], or with the guidance of occlusion-aware modules [36, 71], which have made notable improvements for self-supervised depth estimation using stereo images. However, heavy reliance on context propagation rather than direct matching leaves underlying reliability concerns unresolved. A promising alternative to improve the performance lies in extending the limited stereo viewpoints to a multi-baseline stereo setup. By introducing additional viewpoints along the epipolar line direction, occluded and ill-conditioned regions could poten-

tially gain explicit matching pixels in the extended views. This prompts a critical question: *can we generate reliable multi-baseline stereo images that enhance stereo pairs, enabling more accurate self-supervised depth estimation in these challenging regions?*

To address this, unlike other physical multi-camera systems [30, 32, 53] with multiple baselines, in this paper, we aim to leverage the extensive priors from recent large-scale Latent Diffusion Models (LDMs) [55] and develop the **DMS (Diffusion-based Multi-Baseline Stereo Generation)**, a model-agnostic method that uses geometric priors from LDMs to synthesize novel viewpoints and extend stereo baselines. During training, a Stable Diffusion model is conditioned on either the left or right stereo image and learns to generate the opposite view, guided by simple text prompts "to right" or "to left". During inference, the learned DMS can be used to generate novel views (e.g., *left-left* view by conditioning on the left image with the prompt "to left" or *right-right* view similarly). The proposed DMS effectively extends the baselines of the stereo images and enhances matching information for occluded and out-of-frame regions, thus significantly improving the disparity estimation in these regions. Our experiments indicate that the learned Stable Diffusion model inherently captures depth cues while learning transformations between left and right views, enabling it to generate reliable novel views. Additionally, we found that upscaling the input resolution yields the same pixel-level displacements in generated views, i.e., reduced displacements in original resolution. This allows precise control over shift distances with the scale factor and enables the generation of intermediate view, offering robust supervision signals for self-supervised depth estimation.

Our main contributions lie in three folds:

- We exploit geometric priors within the learned Stable Diffusion model for novel view synthesis along the epipolar line via direction prompts, relying solely on unlabeled stereo image pairs for both training and generation.
- Our synthesized views fill in missing correspondences in ill-posed areas, including occluded regions and out-of-frame regions, providing explicit matching clues for stable photometric-based learning.
- Our proposed **DMS** is a cost-effective, plug-and-play method that enhances self-supervised stereo matching and stereo-supervised monocular depth estimation, achieving state-of-the-art results with up to 35% fewer outliers across multiple benchmarks.

## 2. Related Work

### 2.1. Self-Supervised Depth Estimation

**Self-Supervised Stereo Matching.** With limited access to densely labeled depth data, self-supervised stereo methods have been developed to learn disparity using photo-

metric loss and left-right consistency checks [17, 36, 41, 71, 82, 95]. Early work showed that CNNs could learn stereo matching from photometric cues alone [95], while later methods added modules for handling occlusions [36], parallax attention to capture large disparities [71], and semantic information to refine disparity [82]. Some methods also combine stereo and optical flow estimation to improve the disparity prediction [41].

**Self-Supervised Monocular Depth Estimation with Stereo Supervision.** Self-supervised monocular depth estimation, which is normally trained with monocular video sequences aims to simultaneously estimate the camera poses and predict the scene depths. It has seen significant progress through the use of stereo image pairs, which provide a known relative pose, removing the need for a dedicated pose network like PoseNet. Monodepth [21] introduced this approach by enforcing photometric consistency losses between stereo views, while Monodepth2 [22] improved it with multi-scale depth predictions and auto-masking, achieving greater stability and precision. Building on these foundations, Watson et al. [75] integrated geometric hints to guide learning, and Guizilini et al. [26] employed 3D packing techniques to improve spatial detail and resolution. SDFANet [97] and DiffNet [96] each leverage feature-level information to refine depth predictions, achieving stronger internal consistency and handling of complex scene details.

While current unsupervised depth estimation methods improve reliability in challenging areas such as occluded and out-of-frame regions, they still rely primarily on contextual similarity without explicit geometric cues. In contrast, our proposed DMS incorporates a plug-in tool that harnesses the powerful capabilities of a Stable Diffusion Model to enhance matching information in occluded regions through extended baseline images, significantly advancing disparity estimation where traditional methods encounter limitations.

### 2.2. Multi-Baseline Stereo Image Synthesis

**Geometry-Based Generation.** Previous deep learning-based approaches for novel view generation have primarily relied on geometry-based techniques such as adaptive convolution methods [2, 3, 40, 52, 79], which are often referred to as kernel estimation, where convolutional kernels dynamically adjust based on scene geometry. Deep3D [79] introduces a network that creates probabilistic disparity maps to blend shifted versions of the left-view image, synthesizing a right-view. Niklaus et al. [50] proposed adaptive separable convolutions (SepConv), approximating 2D convolutions with sequential vertical and horizontal 1D kernels for video frame interpolation. Deep3D pan [23] uses a novel T-shaped adaptive kernel with globally and locally adaptive dilation, integrating camera shift and local 3D geometry to synthesize natural 3D panned views from a 2D image.

While these geometry-based methods can produce plausible multi-baseline stereo images, their quality remains low, particularly in challenging ill-posed areas.

**Diffusion Models for Multi-View Synthesis.** Diffusion models [29, 55, 60, 92] have excelled in 2D image generation. Works like DreamFusion [54] and SJC [68] adapted 2D text-to-image models for 3D shape generation, spurring advancements in text-to-3D distillation [1, 9, 10, 31, 38, 57, 58, 65, 73, 76, 88, 99] based on score distillation sampling (SDS) loss. Additionally, several methods [7, 13, 24, 35, 42, 43, 62–64, 66, 74, 77, 87, 90, 98] use 2D diffusion models for multi-view image generation, reconstructing 3D scenes from single images with camera pose prompts. Other approaches [14, 37, 44, 66, 90] apply multi-view diffusion models, leveraging attention layers for image-conditioned novel view synthesis to ensure consistency across views. Most of these methods, however, require multi-view datasets (e.g., Objaverse [12]) for training. In contrast, our proposed DMS is trained solely on original stereo images from stereo datasets, eliminating the need for additional viewpoint information.

### 3. Method

In this section, we first provide an overview of latent diffusion models in Section 3.1. We then present the details of our approach in subsequent sections. As illustrated in Figure 1, the DMS follows a two-stage training framework: multi-baseline stereoscopic view synthesis, followed by self-supervised depth estimation. In Stage 1, we train a Diffusion model to generate multi-baseline views from stereo images. In Stage 2, we use these generated views to train self-supervised depth networks, enhancing disparity estimation through multi-view consistency. Each stage is detailed in Sections 3.2 and Section 3.3.

#### 3.1. Preliminaries

**Latent Diffusion Model.** The Latent Diffusion Model (LDM) [55] substantially refines diffusion models by transitioning their operation into a latent space. This model utilizes an encoder to compress an image  $x$  into a latent representation  $z = E(x)$ , effectively streamlining the learning of the distribution of latent codes, represented as  $z_0 \sim p_{\text{data}}(z_0)$ , consistent with the framework of Denoising Diffusion Probabilistic Models (DDPM) proposed by [29]. LDM operates through a bifurcated process: the forward process methodically adds Gaussian noise across time steps  $t$  to form  $z_t$ , whereas the backward process focuses on noise reduction to more closely approximate the preceding, less noisy state  $z_{t-1}$ . The *forward* process is described as:

$$q(z_t|z_{t-1}) = \mathcal{N}(z_t; \sqrt{1 - \beta_t}z_{t-1}, \beta_t\mathbf{I}), \quad (1)$$

where  $\beta_t$  belonging to  $\{\beta_1, \beta_2, \dots, \beta_T\}$  is the variance scale of the forward process with  $T$  steps.  $\mathcal{N}$  represents the Gaussian

distribution and  $\mathbf{I}$  denotes the unit vector with the same size as the  $z_t$ . In the *backward* process, the conditional denoising model strives to remove the noise and reconstruct the less noisy state  $z_{t-1}$  as follows:

$$p_\theta(z_{t-1}|z_t) = \mathcal{N}(z_{t-1}; \mu_\theta(z_t, t, \tau), \Sigma_\theta(z_t, t, \tau)), \quad (2)$$

where  $\tau$  denotes text embedding,  $\mu_\theta$  and  $\Sigma_\theta$  denote the mean and variance functions derived from the denoising model  $\epsilon_\theta$ , parameterized by  $\theta$ , which characterizes the current state’s statistical properties. In the training phase, the model takes  $z_t$  as the input, which is forwarded from  $z_0$  by  $t$  steps with sampled Gaussian noise  $\epsilon$ . The denoising U-Net estimates the noise  $\hat{\epsilon} = \epsilon_\theta(z_t, t)$ , and the loss function  $\mathcal{L}$  is expressed by:

$$\mathcal{L} = \mathbb{E}_{z_0, \epsilon \sim \mathcal{N}(0,1), t \sim \mathcal{U}(T)} \|\epsilon - \hat{\epsilon}\|^2. \quad (3)$$

Among the prominent LDMs, the Stable Diffusion [55] stands out as a prime example, trained extensively on large-scale image-text pair datasets, showcasing remarkable scalability across various tasks [33, 42, 44].

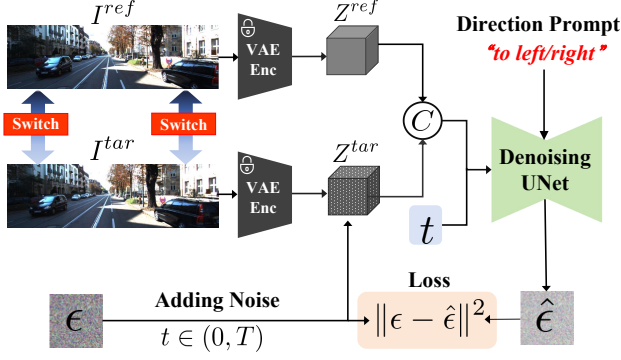
### 3.2. Diffusion-Based Multi-Baseline Stereo Generation (DMS).

#### 3.2.1. Network Architecture

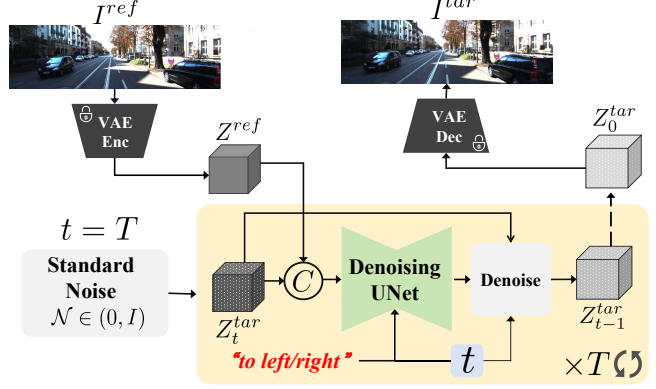
The overall DMS pipeline is illustrated in Figure 2. Similar to [33], we base our model on a pre-trained text-to-image LDM (Stable Diffusion V2), which has been learned from a large number of high-quality images from the LAION-5B [56] dataset. We repurpose the Stable Diffusion model as an image-to-image generator by encoding the reference image as the image prompt, together with the direction text prompt to indicate the transformation direction.

#### 3.2.2. Training Protocol: Direction Prompt Guided Fine-tuning with Stereo Images

As shown in Figure 2.(a), we take the frozen VAE to encode both the reference view  $I_{ref}$  and the target view  $I_{tar}$  to form the latent features  $Z_{ref}$  and  $Z_{tar}$ , respectively. During training, we set the  $I_{ref}$  and  $I_{tar}$  to be either the left or right images and switch step by step. To incorporate scene priors, we condition the denoising U-Net  $\epsilon_\theta$  by concatenating the reference and target latents along the feature dimension, yielding  $Z_{fus}^t = \text{cat}(Z_{ref}^t, Z_{tar}^t)$ . However, relying solely on a reference image is insufficient for determining the direction of transformation, leading to convergence difficulties of the diffusion model. To address this issue, we introduce text-based direction prompts to explicitly define the transformation direction. As shown in Table 3.2.2, we utilize the pre-trained text encoder from the Stable Diffusion model to process simple prompts such as “to right” and “to left”. The resulting text embeddings serve as additional conditioning inputs for the denoising U-Net, enhancing the model’s representation capability. The repurposed



(a) Training Phase of the DMS



(a) Inference Phase of the DMS

Figure 2. **Architecture of the proposed DMS.** (a) In the training phase, we fine-tune the Stable Diffusion model by conditioning it on a reference image ( $l$  or  $r$ ) and a direction prompt specifying the transformation direction to reconstruct the opposite stereo view ( $r$  or  $l$ ). (b) During inference, novel views are iteratively generated from standard Gaussian noise, guided by an input image and a direction prompt.

Table 1. Inference views with different direction text prompts

Input View	Direction Prompt	Target View
Left Image	<i>to left</i>	Left-Left Image ( <b>Novel View</b> )
Left Image	<i>to right</i>	Right Image (Existing View)
Right Image	<i>to left</i>	Left Image (Existing View)
Right Image	<i>to right</i>	Right-Right Image ( <b>Novel View</b> )

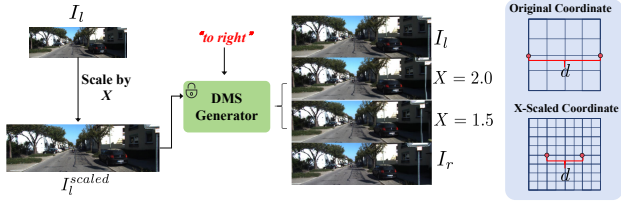


Figure 3. Intermediate view approximation with rescaling operation using pre-trained DMS generator.

denoising process can be described as follows:

$$\epsilon = \epsilon_{\theta}(Z_{ref}^t, Z_{tar}^t, t, \tau_D), \quad (4)$$

here  $\tau_D$  is the direction prompt indicates direction.

### 3.2.3. Inference: Multi-Baseline Stereo Generation

**Extending Stereo Baseline with Direction Prompts.** After training the diffusion model, we utilize it to generate new views with input direction prompts. As shown in Table 3.2.2, beyond the left and right views used for supervision, the fine-tuned diffusion model can generate additional *left-left* and *right-right* views by applying the appropriate direction prompt relative to the reference view. DMS achieves this by inputting the "to left" prompt alongside the left image, using the learned right-to-left transformation to

generate a left-left view. Similarly, applying the reverse prompt enables right-right view synthesis. This technique effectively expands the stereo baseline without additional view supervision, providing a seamless approach to baseline extension.

**Intermediate View Approximation.** While the DMS enables the extension of the stereo baselines, they are limited to fixed baseline units. To enable finer disparity estimation, especially in occluded regions, we propose a simple yet effective method for generating intermediate perspectives with our fine-tuned diffusion model. As illustrated in Figure 3, during the left-to-right generation with the prompt "to right", increasing the input image resolution by a factor  $X > 1$  creates an intermediate view between the left and right perspectives. The horizontal shift ratio follows an inverse relationship with the rescale factor  $X$ , indicating that our fine-tuned diffusion model inherently learns disparity cues through simple left-to-right and right-to-left transformations. Rescaling modifies the image coordinate system, resulting in intermediate views with proportionally smaller horizontal displacements, as shown in Figure 3. Therefore, we leverage this property to generate intermediate views. In our experiments, we set  $X = 2.0$  to approximate a center view and rescale the output back to its original resolution. As shown in Figure 4, we warp the generated views, including intermediate views, onto the left view using ground truth disparity. In Figure 4. (b), the warped images align at the same horizontal positions, demonstrating the geometric consistency of the generated views. We further provide evaluation experiments on the synthesis dataset created by the CARLA [15] simulator to quantitatively assess the quality of the synthesized views. Please refer to the *Supplementary Materials* for more details.



### 3.3. Training of Self-Supervised Depth Estimators

Upon acquiring multi-baseline images, we exploit these novel views to incorporate additional matching cues, thereby improving self-supervised depth estimators. Motivated by [22], we avoid averaging reprojection errors across source images when computing the loss, as it can mislead gradients in occluded regions. Instead, we adopt the *Per-Pixel Minimum Warping Loss* [22] for supervision. This approach is grounded in the straightforward hypothesis that warped source images using accurately predicted disparity or depth may not align with the target image in the occluded or out-of-frame regions, leading to significant photometric errors. In the stereo-matching setups, regions which are visible in the reference view and invisible (occluded) in its right view should be mostly visible in its opposite-side (left) view. By adopting the minimum of losses with multi-baseline warping from both sides, we effectively utilize matching clues from multi-baseline images to optimize disparity in ill-conditioned regions adaptively. The *Per-Pixel Minimum Warping Loss* can be described as follows:

$$\mathcal{L}_{\text{warp}} = \min_{i \in \mathcal{M}} \mathcal{L}_{pe}(I_l, \mathcal{W}(I_i, D \cdot s_i)), \quad (5)$$

$$\mathcal{L}_{pe} = \frac{\alpha}{2} (1 - \text{SSIM}(I_a, I_b)) + (1 - \alpha) \|I_a - I_b\|, \quad (6)$$

where  $\mathcal{M}$  is the scope of source images within the range of  $\{r, ll, rr, c\}$ , representing the *right*, *left-left*, *right-right*, and *center* view, respectively.  $\mathcal{W}$  denotes the warping operation with disparity.  $s_i$  are constant scale factors to scale the disparity for warping the source image to the target left image  $I_l$ . Specifically,  $s_r = 1, s_{ll} = -1, s_{rr} = 2, s_c = 0.5$ . The error metric  $pe$  employs a hybrid loss combining L1 and SSIM [72], following methodologies from [21, 94] for calculating warping errors.

## 4. Experiments

### 4.1. Implementation Details

**Datasets.** To demonstrate the versatility of our proposed DMS model, we trained the diffusion model on various stereo datasets: SceneFlow [47], KITTI 2015 [48], KITTI 2012 [19], and MPI-Sintel [6]. The SceneFlow dataset consists of 39,823 synthetic stereo pairs featuring flying objects with ground truth disparities. MPI-Sintel provides 1,064 synthesized stereo images with ground truth disparities. KITTI 2012 and 2015 provide real-world autonomous driving stereo images with sparse LiDAR-based disparities. **Implementation Details of the Diffusion-Based Multi-Baseline Stereo Generator.** We implement the DMS using Pytorch with 4 NVIDIA A6000 GPUs and utilize the Stable Diffusion V2 [55] as the foundation model. During training, as outlined in Section 3.2.2, we froze the VAE and fine-tuned the Denosing UNet using Adam optimizer with

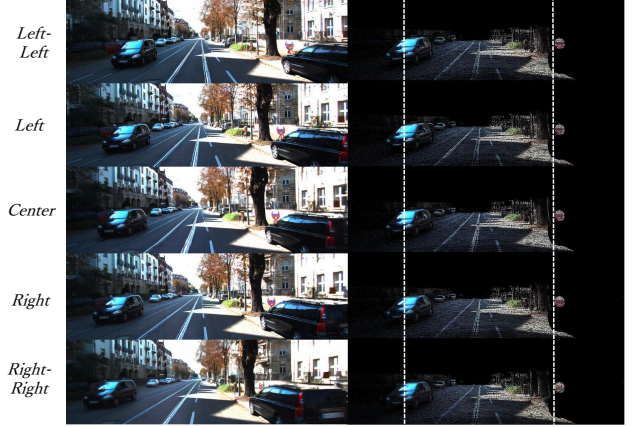


Figure 4. (a) Visualization of generated views on the KITTI dataset. From the top to the bottom: the *left-left*, *left*, *center*, *right*, and *right-right* views. (b) Warped results from each view to the left image view using ground-truth sparse depth are depicted, with a white line marking the same horizontal location for reference.

a constant learning rate of  $2e - 5$  during all training phases with batch size 16. We utilized the DDPM [29] noise scheduler with a total of 1000 steps. During inference, the DDPM sampling was configured to 32 steps for the KITTI dataset and 50 steps for the SceneFlow and MPI-Sintel datasets to ensure the generation quality.

**Implementation Details of the Self-Supervised Depth Networks.** The self-supervised stereo-matching networks are trained on the SceneFlow, KITTI, and MPI-Sintel datasets. For SceneFlow, we utilize the *FlyingThings3D* subset with 19,984 images, excluding highly occluded scenes to ensure viable correspondences. Training is conducted with a batch size of 8 and a cosine decay learning rate starting from  $1e^{-4}$ . For MPI-Sintel, we follow a similar protocol, splitting the dataset for a 9 : 1 evaluation ratio. On KITTI, we fine-tune the SceneFlow pre-trained model for 600 epochs at a resolution of  $320 \times 960$ , with color augmentation as in [81]. Please check *Supplementary Material* for more details. For self-supervised monocular depth estimation with stereo-based supervision, the model is trained on KITTI-Raw and evaluated on the KITTI-eigen [16] split following the pipeline of a previous study [22].

### 4.2. Evaluation of Generated Stereo Images

As reported in Table 2, we evaluate the PSNR and SSIM metrics to assess the quality of DMS-generated stereo views across different datasets. DMS achieves a PSNR of 22–23db on the synthetic SceneFlow dataset and a higher PSNR of 28–29db on the Sintel dataset. To further evaluate our synthesized stereo pairs, we adopt a dual-perspective evaluation inspired by prior work [69, 70], which highlights the importance of both binocular perceptual quality and ge-

Table 2. Evaluation of generation quality on existing stereo perspectives across different datasets. We report the PSNR and SSIM of our generated left and right images via DMS. The "\*" means using the CARLA simulator to test the intermediate views performance.

Metric	SceneFlow [47]		KITTI 2015 [48]		KITTI 2012 [19]		MPI-Sintel [6]		CARLA* [15]				
	Left	Right	Left	Right	Left	Right	Left	Right	Left-Left	Left	Center	Right	Right-Right
<b>PSNR</b> ↑	22.62	22.58	23.60	24.70	23.75	23.74	29.02	28.89	23.63	23.52	21.44	23.06	22.71
<b>SSIM</b> ↑	0.73	0.73	0.80	0.81	0.74	0.75	0.86	0.86	0.76	0.76	0.72	0.75	0.72

Table 3. Quantitative evaluation of stereo image quality on the KITTI 2015 training set. Stereo Perceptual Consistency is measured by Stereo LPIPS (between left/right images) and Fusion SSIM (between grayscale-averaged cyclopean images). Geometric Consistency is assessed by EPE and D1 error from pretrained stereo networks, and photometric Warping Error under ground-truth disparities. † represents that using the official KITTI pre-trained weights.

Input Data	Stereo Perceptual Consistency		Geometric Consistency		
	Stereo LPIPS ↓	Fusion SSIM ↑	Warp Error↓	IGEV-Stereo †[80] EPE↓ / D1↓	NMRF-Stereo †[25] EPE ↓ / D1↓
GT Left + GT Right	0.411	1.00	0.123	0.28 / 0.4	0.36 / 0.5
<b>GT Left + DMS-Gen Right</b>	0.424	0.929	0.138	0.54 / 1.4	0.57 / 1.5

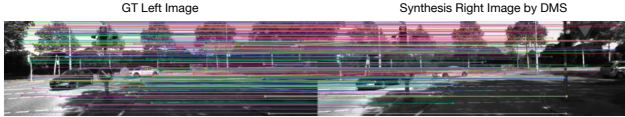


Figure 5. SIFT matches between GT left and DMS-synthesized right images predominantly display horizontal alignments.

ometric consistency. As the original metrics in [69, 70] require non-public implementations and DMOS labels, we instead report simplified proxies. **(1) Stereo Perceptual Consistency:** We compute Stereo LPIPS (between left/right views) and Fusion SSIM (between cyclopean images) as surrogates for binocular realism. **(2) Geometric Consistency:** We use pretrained stereo models [25, 80] to estimate disparity from our synthesized stereo pairs, and report EPE, D1 Error, and Warp Error (under GT disparity). As shown in Table 3, our synthesized right images show strong perceptual alignment with the left view, achieving scores close to GT. The resulting disparity estimates exhibit only a minor drop in accuracy (NMRF Stereo: EPE 0.36→0.57, IGEV Stereo: 0.28→0.54), remaining within the 1-pixel tolerance commonly acceptable in practice. Furthermore, SIFT feature matching between ground truth and synthesized images, illustrated in Figure 5, predominantly shows horizontal and parallel matches, validating the epipolar accuracy of our synthesized images.

Besides, we compare DMS’s performance on the KITTI dataset against state-of-the-art geometry-based multi-baseline synthesis methods, including Deep3D [78], Deep3D Pan [23], and SepConv [51]. Table 4 shows that DMS, trained solely on KITTI Raw, surpasses Deep3D Pan (trained on KITTI and Cityscapes) by approximately 4db

Table 4. Comparisons of novel view synthesis quality on KITTI dataset with geometry-based multi-baseline synthesis methods. The ‘K’ denotes the KITTI dataset, and ‘C’ denotes the Cityscape dataset. **Bold** means the best performance.

Modeling	Training Dataset	PSNR	SSIM
Deep3D [78]	K	20.07	0.637
Deep3D-B [78]	K	20.10	0.633
SepConv [51]	K	19.73	0.633
SepConv-D [51]	K	20.02	0.626
monstet-net(Deep3D pan) [23]	K	20.24	0.641
monstet-net(Deep3D pan) [23]	K + CS	20.76	0.677
<b>DMS(Ours)</b>	K	<b>24.70</b>	<b>0.810</b>

in PSNR and 0.133 in SSIM, underscoring DMS’s superior quality in stereoscopic image synthesis. Additionally, we evaluate DMS performance under ill-posed conditions, with detailed results provided in the *Supplementary Materials*.

### 4.3. Self-Supervised Stereo Matching

#### 4.3.1. Ablation Studies

To validate the effectiveness of the newly generated views by the proposed DMS on self-supervised stereo matching, we carried out ablation studies across various datasets, with results presented in Table 5. We report the End-Point Error (EPE) and outlier ratios (errors>3px) for overall, occluded, and out-of-frame regions to illustrate the efficacy of our method. The occlusion and the out-of-frame masks, which are essential for evaluations, were generated using a left-right consistency check, detailed further in our *Supplementary Material*. For the evaluation of the KITTI 2015 & 2012 dataset, we follow the same strategy used in [95], where we randomly pick 160 image pairs from training set

Table 5. Ablation studies results on SceneFlow, KITTI 2015, and MPI-Sintel datasets, employing PASMnet [71] as the baseline model. The terms *ll*, *rr*, and *c* refer to the *left-left*, *right-right*, and *center* views, respectively. Results include End-Point Error (EPE) and outlier ratios (errors > 3px) across overall, occluded, and out-of-frame regions. **Bold** means the best performance.

Method	SceneFlow[47]						KITTI 2015 [48]						MPI-Sintel [6]					
	EPE↓			>3px%↓			EPE↓			>3px%↓			EPE↓			>3px%↓		
	All	Occ	Oof	All	Occ	Oof	All	Occ	Oof	All	Occ	Oof	All	Occ	Oof	All	Occ	Oof
Baseline	4.09	22.66	10.83	13.5	83.6	42.8	1.48	4.38	9.26	7.7	39.6	64.2	6.34	15.70	14.27	20.1	55.9	66.5
+ <i>ll</i> + <i>rr</i>	2.45	11.45	6.16	9.0	51.0	25.0	1.34	3.83	7.82	6.5	34.4	42.8	5.89	13.56	11.92	19.6	51.6	57.1
+ <i>c</i>	3.75	21.70	7.73	12.5	81.3	38.4	1.36	4.14	7.64	6.7	37.0	49.6	6.30	14.61	<b>11.06</b>	19.1	<b>51.4</b>	<b>52.9</b>
+ <i>ll</i> + <i>rr</i> + <i>c</i>	<b>2.32</b>	<b>11.15</b>	<b>5.57</b>	<b>8.4</b>	<b>49.2</b>	<b>23.4</b>	<b>1.24</b>	<b>3.56</b>	<b>7.31</b>	<b>5.8</b>	<b>32.3</b>	<b>39.7</b>	<b>5.53</b>	<b>13.07</b>	11.40	<b>18.9</b>	<b>51.4</b>	53.0

Table 6. Benchmark results on KITTI 2015 test set. The rows highlighted in gray utilize our proposed DMS. The terms "All" represent overall regions, while "fg" and "all" denote foreground and overall regions, respectively.\* indicates our re-implemented results after unsupervised training with vanilla warping loss and † represents the result using the non-learning-based method where the employment of DMS utilizes multiple image inputs.

Method	All(%) ↓		
	D1-bg	D1-fg	D1-all
<b>Non-Learning Based Method</b>			
SGM† [28]	8.95	20.55	10.88
SGM† + DMS	7.96(11.1% ↓)	16.68(18.8% ↓)	9.41(13.5% ↓)
<b>Learning-Based Methods</b>			
Zhou <i>et.al</i> [95]	-	-	9.91
SegStereo [82]	-	-	8.79
OASM[36]	6.89	19.42	8.98
Flow2Stereo[41]	5.01	14.62	6.61
PASMnet[71]	5.41	16.36	7.23
PASMnet + DMS	5.24(3.1% ↓)	13.96(14.7% ↓)	6.69(7.5% ↓)
StereoNet*[34]	7.31	17.77	9.05
StereoNet* + DMS	4.68(36.0% ↓)	12.06(32.1% ↓)	5.91(34.7% ↓)
CFNet* [59]	7.22	18.54	9.11
CFNet* + DMS	4.64(35.7% ↓)	12.33(33.5% ↓)	5.92(35.0% ↓)
RaftStereo* [39]	3.38	13.62	5.08
RaftStereo* + DMS	2.95(12.7% ↓)	6.88(50.9% ↓)	3.60(29.1% ↓)
IGEVStereo* [80]	3.76	11.14	4.98
IGEVStereo* + DMS	2.80(25.5% ↓)	6.37(45.27% ↓)	3.40(31.72% ↓)
MCStereo* [18]	3.01	13.38	4.73
MCStereo* + DMS	2.83(6.0% ↓)	7.03(47.46% ↓)	3.67(22.41% ↓)

for training, and the other 40 image pairs for validation.

Table 5 illustrates that leveraging novel views generated by the proposed DMS for loss computation markedly improves disparity estimation without modifying the network’s structure, evidenced by improved EPE and D1 values compared to the Baselines. With the proposed DMS, the model exploits geometric consistency across multi-baseline views and get optimized by the multi-view consistency warping loss. This notably improves disparities in occluded regions, with enhancements of 50.8%, 18.7%, and 17.2% on SceneFlow, KITTI, and Sintel datasets, respectively.

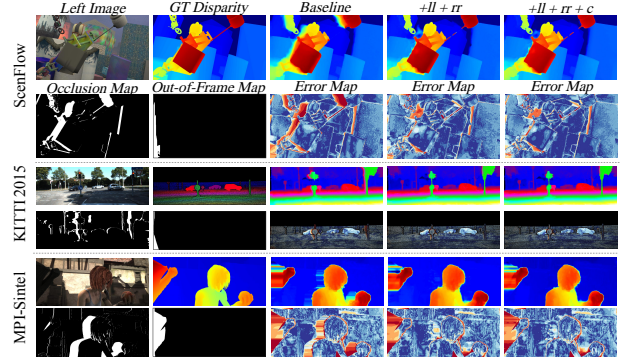


Figure 6. Ablation results on SceneFlow, KITTI 2015, and MPI-Sintel. For each dataset, the first row shows estimated disparities; the second row shows error maps and ill-conditioned regions (e.g., occlusions, out-of-frame areas).

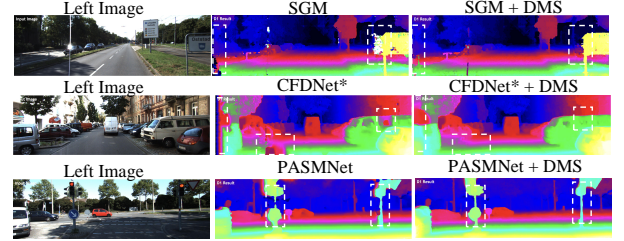


Figure 7. Visualization comparison on KITTI 2015 test set. The proposed DMS significantly improves the disparity estimation at the occluded regions and borders. Zoom in for a better view.

The extended views (*left-left*&*right-right*) generated by the DMS also significantly boost out-of-frame disparity estimation. Figure 6 visually compares these enhancements across datasets, highlighting the Baseline model’s limitations in reconstructing structured disparities, particularly in occluded areas. In contrast, the multi-baseline images from the DMS model enable the model to produce a more accurate reconstruction of structured disparities with reduced errors, underlining the efficacy of our approach in improving geometric precision for stereo-matching tasks.

#### 4.3.2. Evaluation on Self-Supervised Stereo Matching.

Our Diffusion-based Multi-baseline Stereo Generator (DMS) functions as a versatile “plug-in” that leverages ex-



Table 7. Evaluation results on KITTI Eigen test set. The rows highlighted in gray represent the methods that utilize the proposed DMS. “\*” represents a slight modification to model implementation. Refer to *Supplementary Material* for more details.

Method	Abs Rel↓	Sq Rel↓	RMSE↓	RMSE_log↓	A1↑	A2↑	A3↑
MonoDepth [21]	0.120	1.041	5.272	0.217	0.849	0.944	0.974
MonoDepth + DMS	<b>0.109</b>	<b>0.860</b>	<b>5.004</b>	<b>0.202</b>	<b>0.865</b>	<b>0.952</b>	<b>0.978</b>
MonoDepth2 [22]	0.109	0.873	4.960	0.209	0.864	0.948	0.975
MonoDepth2 + DMS	<b>0.105</b>	<b>0.811</b>	<b>4.850</b>	<b>0.200</b>	<b>0.873</b>	<b>0.963</b>	<b>0.988</b>
SDFANet* [97]	0.104	0.997	4.583	0.186	0.888	0.962	0.981
SDFANet* + DMS	<b>0.097</b>	<b>0.643</b>	<b>4.218</b>	<b>0.181</b>	<b>0.891</b>	<b>0.963</b>	<b>0.983</b>
DiffNet [96]	0.104	0.809	4.766	0.201	0.879	0.953	0.976
DiffNet + DMS [96]	<b>0.098</b>	<b>0.726</b>	<b>4.606</b>	<b>0.191</b>	<b>0.886</b>	<b>0.958</b>	<b>0.980</b>

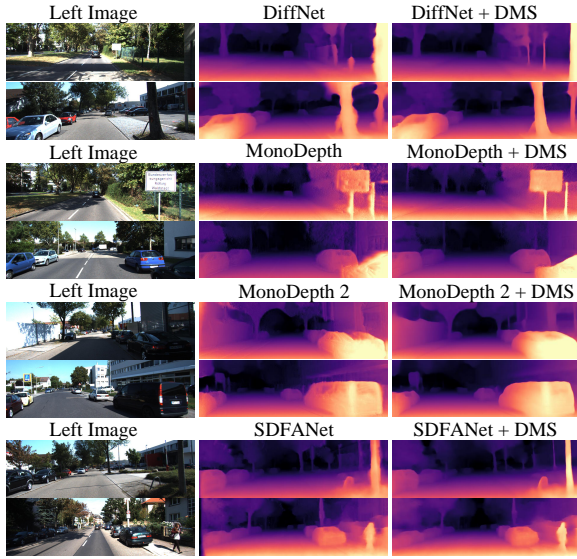


Figure 8. Visualization comparison of self-supervised monocular depth estimations across various existing methods.

isting unlabeled stereo images to train and generate multi-baseline views, allowing for seamless integration into any stereo-matching framework. We further evaluated DMS’s flexibility across various stereo matching networks on the KITTI testing set by fine-tuning a pre-trained SceneFlow model on a mixed KITTI 2012 and 2015 dataset over 600 epochs. For non-learning-based Semi-Global Matching (SGM) [28], we integrate DMS by adapting the cost volume construction with multi-baseline information as detailed in Equation 3.3. As shown in Table 6, the integration into SGM led to substantial improvements, particularly for foreground objects, with a 16.1% improvement in non-occluded regions and an even greater 18.8% improvement across all regions, suggesting high effectiveness in occluded areas though not explicitly evaluated. For learning-based methods, DMS integration significantly enhances performance, with most methods following SGM’s trend and demonstrating its effectiveness in both non-occluded and occluded regions. Additionally, it can further boost the state-of-the-

art supervised methods including RAFTStereo [39] and IGEVStereo [80] and MCStereo [18] for self-supervised fine-tuning on the KITTI dataset. Figure 7 illustrates the improvements of our DMS pipeline for both traditional and learning-based stereo matching methods. Incorporating multi-baseline images leads to significant enhancements in challenging regions, such as occluded and out-of-frame areas, highlighted by white bounding boxes.

#### 4.4. Evaluation on Self-Supervised Monocular Depth Estimation

The primary advantage of our proposed method is its dual capability: the generated multi-baseline image views are useful not only for self-supervised stereo matching but also for improving self-supervised monocular depth estimation. To evaluate this, we extend our DMS framework to monocular depth estimation on the KITTI raw dataset. Following the standard protocol established in [22], we assess performance on the KITTI Eigen test set. Table 7 and Figure 8 demonstrate the effectiveness of integrating the DMS pipeline into existing methods, showing consistent performance improvements across different network architectures. This underscores the broad applicability of DMS in enhancing self-supervised monocular depth estimation.

## 5. Conclusions

In this paper, we have presented DMS, a cost-free model-agnostic approach that exploits geometric priors from large-scale Diffusion models to synthesize novel views across different baselines, thereby supplementing occluded pixels for explicit photometric matching. The proposed DMS synthesizes novel perspectives for the left-left and the right-right baseline camera, along with an intermediate novel view within the original field of vision. Extensive experiments demonstrate that DMS can significantly enhance self-supervised stereo matching and stereo-based monocular depth estimation in a ‘plug-and-play’ manner. The DMS allows leveraging unlabeled stereo images to enhance depth estimation without additional annotations, providing a promising avenue for further advancements in the field.



# DMS: Diffusion-Based Multi-Baseline Stereo Generation for Improving Self-Supervised Depth Estimation

## Supplementary Material

In this supplementary material, we provide additional details and results to complement the main paper. Section 5.1 outlines the experimental setup, including dataset configurations and hyperparameters. Section 5.2 provides more experimental results both in the image quality of the DMS and subsequent training of the self-supervised stereo-matching networks. Finally, in Section 5.3 we illustrate more multi-baseline stereo image results across different datasets using the proposed DMS.

### 5.1. Additional Implementation Details.

#### 5.1.1. Additional Implementation Details of Diffusion-Based Multi-Baseline Stereo Generator (DMS).

In this section, we detail the training process of the Diffusion-based Multi-baseline Stereo Generator (DMS) across various datasets to ensure reproducibility. We implement the DMS using Pytorch with the diffusers [67] as the code base and utilizing the Stable DiffusionV2 [55] as the initial parameter weight. We further report the computation resources that are needed in the inference stage in Table 8.

**SceneFlow.** For training on the SceneFlow dataset, we employ the widely-used FlyingThings3D test set [36, 45, 46, 71, 80, 81, 91] and a training subset of 19,984 images from the FlyingThings3D set, filtering out scenes where occlusion exceeds 80%. To conform to the input size requirements of the Stable Diffusion Model, which necessitates divisibility by 8, the original images are resized from  $540 \times 960$  to  $576 \times 960$  using top padding. We optimize memory usage by employing a batch size of 1 with a gradient accumulation equivalent to a batch size of 16. Optimization is performed using the Adam optimizer with a constant learning rate of  $2e - 5$  under half-precision (float16) settings. The training spans 20 epochs, with the resultant model used for both evaluation and generating new views. Inference utilizes a DDPM scheduler with a step of 50 denoising process for view synthesis. The efficacy of the generated views is quantitatively assessed in Table 2.

**KITTI 2015 & 2012.** For the limited view of the KITTI 2015 and 2012 datasets, we fine-tune the Diffusion model on the KITTI raw dataset [20] which comprises over 43,482 stereo images, where we split the 400 images and 394 images containing in KITTI 2015 and KITTI 2012 dataset and use the left views for training. We pad the original resolution of  $375 \times 1242$  and  $374 \times 1238$  into  $284 \times 1248$  to meet the input size requirements of the Stable Diffusion Model. We use the same optimizer and learning rate that is adopted in training the SceneFlow model and training for

10 epochs to get the final model. Inference utilizes a DDPM scheduler with a step of 32 denoising process for view synthesis. For further used in unsupervised stereo matching, we fine-tune the KITTI-raw pre-trained model on KITTI 2012 and KITTI 2015 datasets, respectively. Note that we both generate views on the KITTI raw dataset for improvement in the performance of monocular depth estimators as outlined in Section 4.4.

**MPI-Sintel Dataset.** For the MPI-Sintel dataset, we partition the dataset into a training set and an evaluation set using a 9 : 1 ratio. The training utilizes the "final pass" images, and we adjust the original resolution from  $436 \times 1024$  to  $440 \times 1024$  to accommodate the model's input requirements. The optimization parameters, including the optimizer and learning rate, are consistent with those used for the SceneFlow model. The training duration is set to 50 epochs to finalize the model. During inference, view synthesis is performed using a DDPM scheduler with a 50-step denoising process.

**CARLA Dataset.** Existing stereo datasets typically contain only *left* and *right* views, making it challenging to evaluate the quality of extended multi-baseline images. To address this, we utilize the CARLA simulator [15] to generate a synthetic multi-baseline stereo dataset with 1000 image pairs (*left*, *center*, *right*, *left-left*, *right-right*) under 15 diverse weather conditions (e.g., *ClearNoon*, *WetNight*). The dataset is split into training and testing sets with a 9:1 ratio. For fine-tuning DMS, we adopt the same training protocol as the KITTI dataset, training for 50 epochs with KITTI pre-trained weights as initialization. During inference, we also utilize a DDPM scheduler with a step of 32 denoising processes for view synthesis. The performance of the generated multi-baseline images can be outlined in Table 10.

#### 5.1.2. Additional Implementation Details of Training the Self-Supervised Depth Estimators.

In this section, we provide a detailed description of the implementation details used for training self-supervised depth networks with multi-baseline images generated by DMS. This includes ablation studies settings and experiments across different datasets on both self-supervised stereo matching and monocular depth estimation.

**Implementation Details of the Ablation Studies.** We leveraged PASMNet [71] as our baseline to evaluate the effectiveness of our multi-baseline stereo images in improving disparity estimation in self-supervised stereo matching settings. We conduct ablation studies on two NVIDIA 3090 GPUs with PyTorch. For the SceneFlow dataset, training

was performed on the FlyThings3D subset (as detailed in Section 5.1.1) and evaluated on the SceneFlow official test set. The model was trained with a batch size of 8, a disparity range of 192, and 100,000 steps. The initial learning rate was set to  $1 \times 10^{-4}$  and reduced using cosine decay. The checkpoint with the lowest End-Point Error (EPE) on the validation set was selected for final evaluation, the results of which are presented in Table 5. Fine-tuning on the KITTI dataset followed the protocol in [95], using 160 image pairs for training and 40 for validation, with weights pre-trained on SceneFlow. The training procedure was consistent with SceneFlow, incorporating data augmentation techniques from [81], such as random cropping and adjustments to brightness, saturation, and contrast. For the Sintel-MPI dataset, the model was trained from scratch using the same parameters as SceneFlow to ensure methodological consistency. This approach validates the robustness of our method across diverse datasets.

**Implementation Details of Training the Self-Supervised Stereo Matching Networks.** Besides the SceneFlow dataset, we further test the performance of the DMS integrated into existing stereo-matching networks to validate the 'plug-in-and-play' ability on the KITTI dataset. For the KITTI 2015 benchmark, we deployed the model which was initially pre-trained on the SceneFlow dataset and subsequently fine-tuned on a combined dataset of KITTI 2012 and 2015, encompassing 394 images. We selected the model with the optimal D1 value for submission to the official KITTI 2015 benchmark to obtain our final results. Considering the limited availability of open-source self-supervised stereo-matching methods, we extended the applicability of our proposed DMS by adapting supervised networks like RaftStereo [39] and IGEVStereo [80] to self-supervised settings using photometric warping loss, demonstrating the method's versatility and broad potential for adaptation.

**Implementation Details of Training the Self-Supervised Monocular Depth Estimators.** All models were trained on the full KITTI Eigen training set (45,200 stereo image pairs) and validated on a small set (4,424 images). We selected models with the lowest validation error and tested them on the KITTI Eigen test set (697 images). For SDFANet [97], marked as \* in the main paper, we made small changes to its original loss computation to incorporate our proposed DMS properly during training. SDFANet predicts a disparity cost volume with shape  $B \times C \times D^* \times H \times W$ , where  $D^*$  is the number of disparity candidates. Disparity is estimated using Soft Argmin on the third dimension. The loss is computed by warping the left image with all disparity candidates, warping each sub-cost of one disparity candidate with shape  $B \times C \times H \times W$  using the corresponding disparity, and calculating a weighted sum to synthesize the right image. The loss is then computed using

the synthesized right image and the input right image. To match other methods and incorporate the proposed DMS, we used the same warping loss as the other three compared methods. We warped the right image to the left using the estimated disparity from SDFANet and computed the loss with the input left image. Similarly, by incorporating DMS, the disparity is used to warp the left-left image, right-right image, and center image to compute additional losses.

### 5.1.3. Evaluation Details of the Self-Supervised Depth Estimations.

**Occlusion and Out-of-Frame Mask Generation for Evaluation.** The MPI-Sintel dataset provides the ground truth occlusion and the out-of-frame mask for evaluation, but SceneFlow and KITTI did not provide such specific masks for evaluation. To address this issue, we use the same strategy used in [46] by using the left-right consistency to generate the occlusion mask and the ground disparity to calculate the out-of-frame mask. The process can be described as follows:

$$M_{occ} = \begin{cases} 1 & \text{if } D_{\Delta}(x, y) \geq 1, \\ 0 & \text{otherwise,} \end{cases} \quad (7)$$

$$M_{oof} = \begin{cases} 1 & \text{if } D_{shift}(x, y) < 0, \\ 0 & \text{otherwise,} \end{cases} \quad (8)$$

$$D_{\Delta}(x, y) = |d_l(x, y) - d_r(x + d_l(x, y), y)|, \quad (9)$$

$$D_{shift}(x, y) = x - d_l(x, y), \quad (10)$$

where  $M_{occ}$  and  $M_{oof}$  represents the generated occlusion masks and the out-of-frame mask, respectively. And the  $d_l$  and  $d_r$  are the ground truth disparity map. For the reason that the KITTI dataset only provides the ground-truth sparse disparity maps for the left images, which makes it difficult to directly apply the left-right consistency check to generate the occlusion masks, following the strategy utilized in [46], we use a pre-trained model [11] to generate the pseudo-left and pseudo-left disparities, the left-right consistency check between the pseudo disparity maps for the left view and the right view is applied to generate a pseudo occlusion mask for performance evaluation.

**Evaluation Metrics for Self-Supervised Stereo Matching.** To showcase the effectiveness of our proposed DMS, especially on ill-conditioned regions, we report the End-Point-Error (EPE) and the  $> 3px$  outliers (percentage of the error bigger than 3 pixels) on overall regions, the occluded regions, and out-of-frame regions, respectively. The definition of the EPE is as follows:

$$EPE(d, \hat{d}) = |d - \hat{d}|. \quad (11)$$

For the performance on the KITTI 2015 validation set, we report the  $> 3px$  which describes the outlier ratio of the

Table 8. Computation resources for utilizing the DMS to generate multi-baseline stereo images across different datasets with different resolutions. Note the inference time and GPU Memory are tested on a single NVIDIA A6000 GPU.

Dataset	Denoising Steps	Inference Time Per Image	GPU Memory
SceneFlow [47]	50	5.34 s	7.61 G
KITTI [19]	32	4.12 s	6.82 G
MPI-Sintel [6]	50	6.04 s	6.72 G
CARLA [15]	32	4.30 s	7.05G

predicted disparity. where can be described as follows:

$$> 3px = \frac{N_{\Delta e > 3px}}{N_{total}}, \quad \Delta e = |d - \hat{d}|, \quad (12)$$

where  $N$  means the number of pixels.

For the KITTI 2015 testing benchmark, we follow the official evaluation protocol to report the D1-value as shown in Table 6.

**Evaluation Metrics for Self-Supervised Monocular Depth Estimation.** We evaluate each method using several metrics from prior work [16], which uses the predicted depth  $d^*$  and GT depth  $\hat{d}^*$  in meters to compute the errors:

$$AbsRel = \frac{1}{|T|} \sum_{d^* \in T} \frac{|d^* - \hat{d}^*|}{\hat{d}^*}, \quad (13)$$

$$SqRel = \frac{1}{|T|} \sum_{d^* \in T} \frac{\|d^* - \hat{d}^*\|^2}{\hat{d}^*}, \quad (14)$$

$$RMSE = \sqrt{\frac{1}{|T|} \sum_{d^* \in T} \|d^* - \hat{d}^*\|^2}, \quad (15)$$

$$RMSE(\log) = \sqrt{\frac{1}{|T|} \sum_{d^* \in T} \|\log d^* - \log \hat{d}^*\|^2}, \quad (16)$$

$$A(thr) = \max\left(\frac{d_i^*}{\hat{d}_i^*}, \frac{\hat{d}_i^*}{d_i^*}\right) = \delta < thr, \quad (17)$$

where  $T$  denotes all the test pixels in all test image samples, and A1, A2, A3 denote the  $thr$  be set as 1.25, 1.25<sup>2</sup>, and 1.25<sup>3</sup> respectively.

## 5.2. Addition Experimental Results.

In addition to the experimental results presented in the main paper, this section provides supplementary evaluations to thoroughly demonstrate the validity of our proposed Diffusion-Based Multi-Baseline Stereo Generation (DMS) and its impact on improving the performance of self-supervised depth estimation methods.

### 5.2.1. Diffusion-Based Multi-Baseline Stereo Generation

**More Ablations on Rescale-Factor  $X$ .** We select a rescale-factor of 2.0 in the paper as the *center* view provides the

Table 9. Additional ablations on the KITTI2015 validation set with varying rescale factors. \*Generate left-left and right-right images with a 0.5 scale.

Factor $X$	Views Used	EPE↓			D1↓		
		All	Occ	Oof	All	Occ	Oof
-	$l, r$	1.48	4.38	9.26	7.7	39.6	64.2
0.5	$+ ll * + rr *$	1.37	3.97	7.90	6.8	36.1	48.0
1.0	$+ ll + rr$	1.34	3.83	7.82	6.5	34.4	42.8
1.5	$+ \frac{2}{3} l \rightarrow r$	1.40	4.22	8.17	7.1	38.1	51.7
2.0	$+ c$	1.36	4.14	7.64	6.7	37.0	49.6
3.0	$+ \frac{1}{3} l \rightarrow r$	1.41	4.16	8.33	7.1	36.7	52.9
All Above	$+ all$	1.22	3.44	7.20	5.6	31.7	39.3

most effective representation of the intermediate view between left and right images. To further justify this choice, we extend the ablation studies in Table 9 with additional candidates (0.5, 1.5, 3.0), as shown in Table.1 below. These factors produce denser intermediate views, such as  $\frac{1}{3} l \rightarrow r$  and  $\frac{2}{3} l \rightarrow r$ , improving performance over the baseline. However, the most effective configurations remain the default left-left ( $+ll$ ), right-right ( $+rr$ ), and center view ( $+c$ ), highlighted in gray, which cover most out-of-view and occluded regions. Moreover, applying all new views together further improves overall EPE to 1.22, closely matching the 1.24 achieved with only  $+ll+rr+c$ . Considering both performance and efficiency, we chose a rescale-factor of 2.0 for intermediate view generation in the paper.

**Computation Resources Analysis.** We report the computation resources for utilizing the DMS to generate multi-baseline stereo images using an NVIDIA A6000 GPU and Intel i9-13900KF CPU. The image resolutions for inference are  $540 \times 960$ ,  $384 \times 1280$ ,  $436 \times 1024$ , and  $540 \times 960$  for SceneFlow, KITTI, MPI-Sintel, and CARLA datasets, respectively. This demonstrates that our DMS can efficiently perform inference on a single GPU with less than 8GB of memory, highlighting its practical applicability.

### Multi-Baseline Stereo Image Evaluation on CARLA.

Stereo datasets typically provide only *left* and *right* views, limiting the evaluation of extended multi-baseline images. To address this, we generate a synthetic multi-baseline stereo dataset using the CARLA simulator [15], consisting of 1000 image pairs (*left*, *center*, *right*, *left-left*, *right-right*) across 15 weather conditions (e.g., *ClearNoon*, *WetNight*). During training, we also only used the left and right view to train the DMS and used the pre-trained DMS model to generate multi-baseline stereo images. As shown in Table 10, we report the PSNR and SSIM of the generated views including the novel view left-left, right-right, and center view, respectively. The check-marked annotations indicate the newly generated perspectives (left-left and right-right) obtained using our proposed inference method. These views exhibit the comparable performance of PSNR and SSIM to

Table 10. Novel view quality evaluations on synthesis dataset created by CARLA [15] simulator. We report the PSNR and SSIM for both the left view, right view, left-left view, right-right view, and center view, respectively.

Generated View	Input View	Direction Prompt	Upscaling	Novel View	PSNR	SSIM
Left	Right	<i>to left</i>	-		23.52	0.76
Right	Left	<i>to right</i>	-		23.06	0.75
Left-Left	Left	<i>to left</i>	-	✓	23.63	0.76
Right-Right	Right	<i>to right</i>	-	✓	22.71	0.72
Center	Left	<i>to right</i>	×2	✓	21.44	0.72

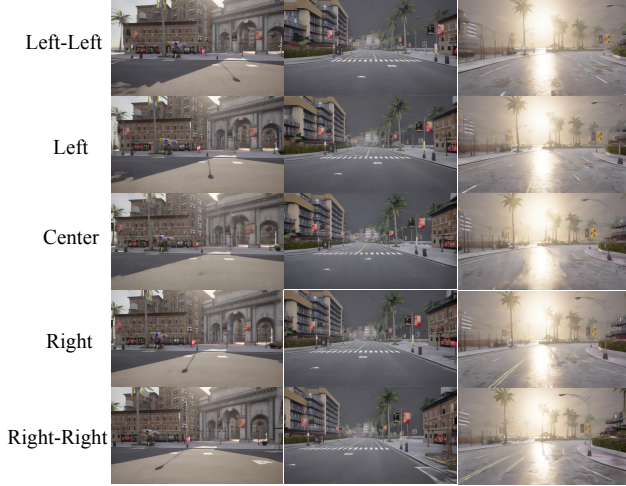


Figure 9. Multi-baseline stereo images generation using proposed DMS on the CARLA synthesis dataset.

the rendered left and right views, despite the absence of ground truth left-left and right-right views during training. While the generated intermediate views show a slight decrease in PSNR, their SSIM remains consistent with other views. This demonstrates that the multi-baseline images produced by DMS maintain geometric consistency, making them valuable for improving self-supervised depth estimation. Further visualization results are illustrated in Section 5.2.2 in this supplementary material.

### 5.2.2. Self-Supervised Stereo Matching

In addition to the ablation studies presented in the main paper, we further evaluated the impact of multi-baseline stereo images generated by our DMS on self-supervised stereo-matching performance using the KITTI 2012 dataset. Same as the main paper, we also use PASMNet [71] as the baseline for self-supervised stereo-matching training.

As detailed in Table 11, the results show that adding *ll* and *rr* significantly reduces both EPE and outlier ratios in all regions compared to the baseline, particularly improving occluded and out-of-frame areas. Further incorporating the center view (*c*) yields the best performance, achieving

Table 11. Ablation Studies On KITTI 2012 dataset for self-supervised stereo matching. The terms *ll*, *rr*, and *c* refer to the left-left, right-right, and center views, respectively. Results include End-Point Error (EPE) and outlier ratios (errors > 3px) across general, occluded, and out-of-frame regions. "Occ" and "Oof" represent the occluded regions and the out-of-frame regions, respectively.

Method	KITTI 2012					
	EPE↓			>3px(%)↓		
	All	Occ	Oof	All	Occ	Oof
Baseline	1.44	5.01	15.58	7.5	40.0	66.3
+ <i>ll</i> + <i>rr</i>	1.24	4.58	10.65	6.0	37.7	53.4
+ <i>c</i>	1.41	4.96	14.83	6.8	40.1	65.6
+ <i>ll</i> + <i>rr</i> + <i>c</i>	1.16	4.39	9.77	5.81	36.1	51.4



Figure 10. Multi-baseline stereo images generation using proposed DMS on the KITTI 2015 dataset.

the lowest EPE and outlier percentages, demonstrating the effectiveness of multi-baseline integration in enhancing geometric consistency and depth estimation robustness.

### 5.3. Additional Visualization Results.

#### 5.3.1. Multi-Baseline Stereo Image Generation Results Visualization.

Figure 10, Figure 11, Figure 12, and Figure 9 showcase additional visualizations of the proposed DMS model applied to the SceneFlow, KITTI, MPI-Sintel, and CARLA datasets. These figures illustrate the model's capability to synthesize novel views along the epipolar line, leveraging



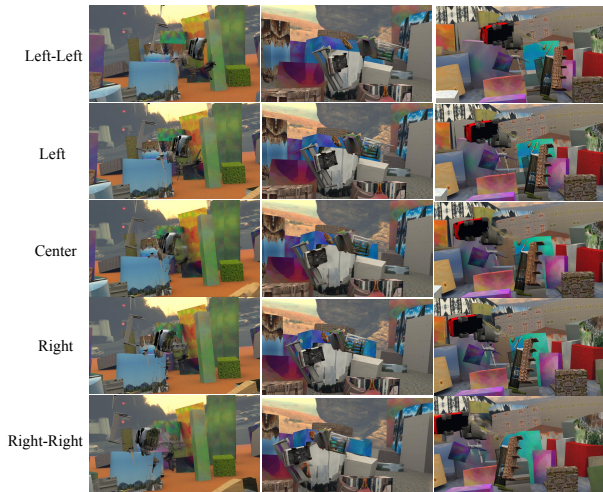


Figure 11. Multi-baseline stereo images generation using proposed DMS on the SceneFlow dataset.



Figure 12. Multi-baseline stereo images generation using proposed DMS on the MPI-Sintel dataset.

directional prompts to extend stereo baselines. The results highlight the versatility and robustness of DMS in handling diverse scenarios, from highly controlled synthetic datasets to complex real-world environments, while maintaining geometric consistency.

## References

- [1] Mohammadreza Armandpour, Huangjie Zheng, Ali Sadeghian, Amir Sadeghian, and Mingyuan Zhou. Re-imagine the negative prompt algorithm: Transform 2d diffusion into 3d, alleviate janus problem and beyond. *arXiv preprint arXiv:2304.04968*, 2023. 3
- [2] Juan Luis Gonzalez Bello and Munchurl Kim. Deep 3d-zoom net: Unsupervised learning of photo-realistic 3d-zoom. *arXiv preprint arXiv:1909.09349*, 2019. 2
- [3] Juan Luis Gonzalez Bello and Munchurl Kim. Deep 3d pan via local adaptive” t-shaped” convolutions with global and local adaptive dilations. In *International Conference on Learning Representations*, 2020. 2
- [4] Shariq Farooq Bhat, Reiner Birkel, Diana Wofk, Peter Wonka, and Matthias Müller. Zoedepth: Zero-shot transfer by combining relative and metric depth. *arXiv preprint arXiv:2302.12288*, 2023. 1
- [5] Aleksei Bochkovskii, Amaël Delaunoy, Hugo Germain, Marcel Santos, Yichao Zhou, Stephan R Richter, and Vladlen Koltun. Depth pro: Sharp monocular metric depth in less than a second. *arXiv preprint arXiv:2410.02073*, 2024. 1
- [6] D. J. Butler, J. Wulff, G. B. Stanley, and M. J. Black. A naturalistic open source movie for optical flow evaluation. In *Proc. Eur. Conf. Comp. Vis.*, pages 611–625. Springer-Verlag, 2012. 5, 6, 7, 3
- [7] Eric R Chan, Koki Nagano, Matthew A Chan, Alexander W Bergman, Jeong Joon Park, Axel Levy, Miika Aittala, Shalini De Mello, Tero Karras, and Gordon Wetzstein. Generative novel view synthesis with 3d-aware diffusion models. In *ICCV*, 2023. 3
- [8] J. Chang and Y. Chen. Pyramid stereo matching network. In *Proc. IEEE Conf. Comp. Vis. Patt. Recogn.*, pages 5410–5418, 2018. 1
- [9] Rui Chen, Yongwei Chen, Ningxin Jiao, and Kui Jia. Fantasia3d: Disentangling geometry and appearance for high-quality text-to-3d content creation. *arXiv preprint arXiv:2303.13873*, 2023. 3
- [10] Yiwen Chen, Chi Zhang, Xiaofeng Yang, Zhongang Cai, Gang Yu, Lei Yang, and Guosheng Lin. It3d: Improved text-to-3d generation with explicit view synthesis. *arXiv preprint arXiv:2308.11473*, 2023. 3
- [11] Xuelian Cheng, Yiran Zhong, Mehrtash Harandi, Yuchao Dai, Xiaojun Chang, Hongdong Li, Tom Drummond, and Zongyuan Ge. Hierarchical neural architecture search for deep stereo matching. *Advances in neural information processing systems*, 33:22158–22169, 2020. 2
- [12] Matt Deitke, Dustin Schwenk, Jordi Salvador, Luca Weihs, Oscar Michel, Eli VanderBilt, Ludwig Schmidt, Kiana Ehsani, Aniruddha Kembhavi, and Ali Farhadi. Objaverse: A universe of annotated 3d objects. In *Proceedings of the IEEE/CVF Conference on Computer Vision and Pattern Recognition*, pages 13142–13153, 2023. 3
- [13] Congyue Deng, Chiyu Jiang, Charles R Qi, Xinchun Yan, Yin Zhou, Leonidas Guibas, Dragomir Anguelov, et al. Nerdi: Single-view nerf synthesis with language-guided diffusion as general image priors. In *CVPR*, 2023. 3
- [14] Zijun Deng, Xiangteng He, Yuxin Peng, Xiongwei Zhu, and Lele Cheng. Mv-diffusion: Motion-aware video diffusion model. In *Proceedings of the 31st ACM International Conference on Multimedia*, pages 7255–7263, 2023. 3
- [15] Alexey Dosovitskiy, German Ros, Felipe Codevilla, Antonio Lopez, and Vladlen Koltun. Carla: An open urban driving simulator. In *Conference on robot learning*, pages 1–16. PMLR, 2017. 4, 6, 1, 3
- [16] David Eigen, Christian Puhrsch, and Rob Fergus. Depth map prediction from a single image using a multi-scale deep network. *Advances in neural information processing systems*, 27, 2014. 5, 3

- [17] Xiule Fan, Soo Jeon, and Baris Fidan. Occlusion-aware self-supervised stereo matching with confidence guided raw disparity fusion. In *2022 19th Conference on Robots and Vision (CRV)*, pages 132–139, 2022. 1, 2
- [18] Miaojie Feng, Junda Cheng, Hao Jia, Longliang Liu, Gangwei Xu, and Xin Yang. Mc-stereo: Multi-peak lookup and cascade search range for stereo matching. In *2024 International Conference on 3D Vision (3DV)*, pages 344–353. IEEE, 2024. 7, 8
- [19] Andreas Geiger, Philip Lenz, and Raquel Urtasun. Are we ready for autonomous driving? the kitti vision benchmark suite. In *Proc. IEEE Conf. Comp. Vis. Patt. Recogn.*, pages 3354–3361. IEEE, 2012. 5, 6, 3
- [20] Andreas Geiger, Philip Lenz, Christoph Stiller, and Raquel Urtasun. Vision meets robotics: The kitti dataset. *International Journal of Robotics Research (IJRR)*, 2013. 1
- [21] Clément Godard, Oisín Mac Aodha, and Gabriel J Brostow. Unsupervised monocular depth estimation with left-right consistency. In *Proc. IEEE Conf. Comp. Vis. Patt. Recogn.*, pages 270–279, 2017. 2, 5, 8
- [22] Clément Godard, Oisín Mac Aodha, Michael Firman, and Gabriel J Brostow. Digging into self-supervised monocular depth estimation. In *Proc. IEEE Int. Conf. Comp. Vis.*, pages 3828–3838, 2019. 2, 5, 8
- [23] Juan Luis Gonzalez Bello and Munchurl Kim. Deep 3d pan via local adaptive” t-shaped” convolutions with global and local adaptive dilations. In *International Conference on Learning Representations, ICLR 2020*, pages 1–20. 2020 International Conference on Learning Representations, 2020. 2, 6
- [24] Jiatao Gu, Alex Trevithick, Kai-En Lin, Joshua M Susskind, Christian Theobalt, Lingjie Liu, and Ravi Ramamoorthi. Nerfdiff: Single-image view synthesis with nerf-guided distillation from 3d-aware diffusion. In *ICML*, 2023. 3
- [25] Tongfan Guan, Chen Wang, and Yun-Hui Liu. Neural markov random field for stereo matching. In *Proceedings of the IEEE/CVF Conference on Computer Vision and Pattern Recognition*, pages 5459–5469, 2024. 6
- [26] Vitor Guizilini, Rares Ambrus, Sudeep Pillai, Allan Raventos, and Adrien Gaidon. 3d packing for self-supervised monocular depth estimation. In *Proceedings of the IEEE/CVF conference on computer vision and pattern recognition*, pages 2485–2494, 2020. 2
- [27] X. Guo, K. Yang, W. Yang, X. Wang, and H. Li. Group-wise correlation stereo network. In *Proc. IEEE Conf. Comp. Vis. Patt. Recogn.*, pages 3268–3277, 2019. 1
- [28] Heiko Hirschmüller. Stereo processing by semiglobal matching and mutual information. *IEEE Trans. Pattern Anal. Mach. Intell.*, 30(2):328–341, 2007. 7, 8
- [29] Jonathan Ho, Ajay Jain, and Pieter Abbeel. Denoising diffusion probabilistic models. *Proc. Advances in Neural Inf. Process. Syst.*, 33:6840–6851, 2020. 3, 5
- [30] Dominik Honegger, Torsten Sattler, and Marc Pollefeys. Embedded real-time multi-baseline stereo. In *2017 IEEE International Conference on Robotics and Automation (ICRA)*, pages 5245–5250, 2017. 2
- [31] Yukun Huang, Jianan Wang, Yukai Shi, Xianbiao Qi, Zheng-Jun Zha, and Lei Zhang. Dreamtime: An improved optimization strategy for text-to-3d content creation. *arXiv preprint arXiv:2306.12422*, 2023. 3
- [32] Saad Imran, Muhammad Umar Karim Khan, Sikander Mukaram, and Chong-Min Kyung. Unsupervised monocular depth estimation with multi-baseline stereo. In *Proc. British Machine Vis. Conf.*, 2020. 2
- [33] Bingxin Ke, Anton Obukhov, Shengyu Huang, Nando Metzger, Rodrigo Caye Daudt, and Konrad Schindler. Repurposing diffusion-based image generators for monocular depth estimation. In *Proc. IEEE Conf. Comp. Vis. Patt. Recogn.*, 2024. 3
- [34] Sameh Khamis, Sean Fanello, Christoph Rhemann, Adarsh Kowdle, Julien Valentin, and Shahram Izadi. Stereonet: Guided hierarchical refinement for real-time edge-aware depth prediction. In *Proc. Eur. Conf. Comp. Vis.*, pages 573–590, 2018. 7
- [35] Jiabao Lei, Jiapeng Tang, and Kui Jia. Generative scene synthesis via incremental view inpainting using rgbd diffusion models. In *CVPR*, 2022. 3
- [36] Ang Li and Zejian Yuan. Occlusion aware stereo matching via cooperative unsupervised learning. In *Proc. Asian Conf. Comp. Vis.*, pages 197–213. Springer, 2018. 1, 2, 7
- [37] Peng Li, Yuan Liu, Xiaoxiao Long, Feihu Zhang, Cheng Lin, Mengfei Li, Xingqun Qi, Shanghang Zhang, Wenhan Luo, Ping Tan, et al. Era3d: High-resolution multiview diffusion using efficient row-wise attention. *arXiv preprint arXiv:2405.11616*, 2024. 3
- [38] Chen-Hsuan Lin et al. Magic3d: High-resolution text-to-3d content creation. *arXiv preprint arXiv:2302.01335*, 2023. 3
- [39] Lahav Lipson, Zachary Teed, and Jia Deng. Raft-stereo: Multilevel recurrent field transforms for stereo matching. In *2021 International Conference on 3D Vision (3DV)*, pages 218–227. IEEE, 2021. 7, 8, 2
- [40] Miaomiao Liu, Xuming He, and Mathieu Salzmann. Geometry-aware deep network for single-image novel view synthesis. In *Proceedings of the IEEE Conference on Computer Vision and Pattern Recognition*, pages 4616–4624, 2018. 2
- [41] Pengpeng Liu, Irwin King, Michael R Lyu, and Jia Xu. Flow2stereo: Effective self-supervised learning of optical flow and stereo matching. In *Proc. IEEE Conf. Comp. Vis. Patt. Recogn.*, pages 6648–6657, 2020. 2, 7
- [42] Ruoshi Liu, Rundi Wu, Basile Van Hoorick, Pavel Tokmakov, Sergey Zakharov, and Carl Vondrick. Zero-1-to-3: Zero-shot one image to 3d object, 2023. 3
- [43] Xinhang Liu, Shiu-hong Kao, Jiaben Chen, Yu-Wing Tai, and Chi-Keung Tang. Deceptive-nerf: Enhancing nerf reconstruction using pseudo-observations from diffusion models. *arXiv preprint arXiv:2305.15171*, 2023. 3
- [44] Yuan Liu, Cheng Lin, Zijiao Zeng, Xiaoxiao Long, Lingjie Liu, Taku Komura, and Wenping Wang. Syncdreamer: Generating multiview-consistent images from a single-view image. *arXiv preprint arXiv:2309.03453*, 2023. 3
- [45] Zihua Liu, Songyan Zhang, Zhicheng Wang, and Masatoshi Okutomi. Digging into normal incorporated stereo match-

- ing. In *Proc. ACM Int. Conf. Multimedia*, pages 6050–6060, 2022. 1
- [46] Zihua Liu, Yizhou Li, and Masatoshi Okutomi. Global occlusion-aware transformer for robust stereo matching. In *Proc. Winter Conf. on Appl. of Comp. Vis.*, pages 3535–3544, 2024. 1, 2
- [47] Nikolaus Mayer, Eddy Ilg, Philip Hausser, Philipp Fischer, Daniel Cremers, Alexey Dosovitskiy, and Thomas Brox. A large dataset to train convolutional networks for disparity, optical flow, and scene flow estimation. In *Proc. IEEE Conf. Comp. Vis. Patt. Recogn.*, pages 4040–4048, 2016. 5, 6, 7, 3
- [48] Moritz Menze and Andreas Geiger. Object scene flow for autonomous vehicles. In *Proc. IEEE Conf. Comp. Vis. Patt. Recogn.*, pages 3061–3070, 2015. 5, 6, 7
- [49] Don Murray and James J Little. Using real-time stereo vision for mobile robot navigation. *Autonomous Robots*, 8:161–171, 2000. 1
- [50] Alex Nichol et al. Glide: Towards photorealistic image generation and editing with text-guided diffusion models. *arXiv preprint arXiv:2112.10741*, 2021. 2
- [51] Simon Niklaus, Long Mai, and Feng Liu. Video frame interpolation via adaptive separable convolution. In *Proceedings of the IEEE international conference on computer vision*, pages 261–270, 2017. 6
- [52] Simon Niklaus, Long Mai, and Feng Liu. Video frame interpolation via adaptive separable convolution. In *Proceedings of the IEEE international conference on computer vision*, pages 261–270, 2017. 2
- [53] Masatoshi Okutomi and Takeo Kanade. A multiple-baseline stereo. *IEEE Transactions on pattern analysis and machine intelligence*, 15(4):353–363, 1993. 2
- [54] Ben Poole, Ajay Jain, Pieter Abbeel, et al. Dreamfusion: Text-to-3d using 2d diffusion models. *arXiv preprint arXiv:2209.14988*, 2022. 3
- [55] Robin Rombach, Andreas Blattmann, Dominik Lorenz, Patrick Esser, and Björn Ommer. High-resolution image synthesis with latent diffusion models. In *Proc. IEEE Conf. Comp. Vis. Patt. Recogn.*, pages 10684–10695, 2022. 2, 3, 5, 1
- [56] Christoph Schuhmann, Romain Beaumont, Richard Vencu, Cade Gordon, Ross Wightman, Mehdi Cherti, Theo Coombes, Aarush Katta, Clayton Mullis, Mitchell Wortsman, et al. Laion-5b: An open large-scale dataset for training next generation image-text models. *Advances in Neural Information Processing Systems*, 35:25278–25294, 2022. 3
- [57] Hoigi Seo, Hayeon Kim, Gwanghyun Kim, and Se Young Chun. Ditto-nerf: Diffusion-based iterative text to omnidirectional 3d model. *arXiv preprint arXiv:2304.02827*, 2023. 3
- [58] Junyoung Seo, Wooseok Jang, Min-Seop Kwak, Jaehoon Ko, Hyeonsu Kim, Junho Kim, Jin-Hwa Kim, Jiyoung Lee, and Seungryong Kim. Let 2d diffusion model know 3d-consistency for robust text-to-3d generation. *arXiv preprint arXiv:2303.07937*, 2023. 3
- [59] Zhelun Shen, Yuchao Dai, and Zhibo Rao. Cfnets: Cascade and fused cost volume for robust stereo matching. In *Proc. IEEE Conf. Comp. Vis. Patt. Recogn.*, pages 13906–13915, 2021. 7
- [60] Jiaming Song, Chenlin Meng, and Stefano Ermon. Denoising diffusion implicit models. *arXiv preprint arXiv:2010.02502*, 2020. 3
- [61] Hideyuki Suenaga, Huy Hoang Tran, Hongen Liao, Ken Masamune, Takeyoshi Dohi, Kazuto Hoshi, and Tsuyoshi Takato. Vision-based markerless registration using stereo vision and an augmented reality surgical navigation system: a pilot study. *BMC Medical Imaging*, 15(1):1–11, 2015. 1
- [62] Stanislaw Szymanowicz, Christian Rupprecht, and Andrea Vedaldi. Viewset diffusion: (0-) image-conditioned 3d generative models from 2d data. *arXiv preprint arXiv:2306.07881*, 2023. 3
- [63] Shitao Tang, Fuyang Zhang, Jiacheng Chen, Peng Wang, and Yasutaka Furukawa. Mvdifffusion: Enabling holistic multi-view image generation with correspondence-aware diffusion. *arXiv preprint arXiv:2307.01097*, 2023.
- [64] Ayush Tewari, Tianwei Yin, George Cazenavette, Semon Rezhchikov, Joshua B Tenenbaum, Frédo Durand, William T Freeman, and Vincent Sitzmann. Diffusion with forward models: Solving stochastic inverse problems without direct supervision. *arXiv preprint arXiv:2306.11719*, 2023. 3
- [65] Christina Tsalicoglou, Fabian Manhardt, Alessio Tonioni, Michael Niemeyer, and Federico Tombari. Textmesh: Generation of realistic 3d meshes from text prompts. *arXiv preprint arXiv:2304.12439*, 2023. 3
- [66] Hung-Yu Tseng, Qinbo Li, Changil Kim, Suhub Alsisan, Jia-Bin Huang, and Johannes Kopf. Consistent view synthesis with pose-guided diffusion models. In *CVPR*, 2023. 3
- [67] Patrick von Platen, Suraj Patil, Anton Lozhkov, Pedro Cuenca, Nathan Lambert, Kashif Rasul, Mishig Davaadorj, Dhruv Nair, Sayak Paul, William Berman, Yiyi Xu, Steven Liu, and Thomas Wolf. Diffusers: State-of-the-art diffusion models. <https://github.com/huggingface/diffusers>, 2022. 1
- [68] Haochen Wang, Xiaodan Du, Jiahao Li, Raymond A Yeh, and Greg Shakhnarovich. Score jacobian chaining: Lifting pretrained 2d diffusion models for 3d generation. In *CVPR*, 2023. 3
- [69] Jiheng Wang, Abdul Rehman, Kai Zeng, Shiqi Wang, and Zhou Wang. Quality prediction of asymmetrically distorted stereoscopic 3d images. *IEEE Transactions on Image Processing*, 24(11):3400–3414, 2015. 5, 6
- [70] Jiheng Wang, Shiqi Wang, Kede Ma, and Zhou Wang. Perceptual depth quality in distorted stereoscopic images. *IEEE Transactions on Image Processing*, 26(3):1202–1215, 2016. 5, 6
- [71] Longguang Wang, Yulan Guo, Yingqian Wang, Zhengfa Liang, Zaiping Lin, Jungang Yang, and Wei An. Parallax attention for unsupervised stereo correspondence learning. *IEEE Trans. Pattern Anal. Mach. Intell.*, 44(4):2108–2125, 2020. 1, 2, 7, 4
- [72] Zhou Wang, Alan C Bovik, Hamid R Sheikh, and Eero P Simoncelli. Image quality assessment: from error visibility to structural similarity. *IEEE Trans. Image Process.*, 13(4):600–612, 2004. 5
- [73] Zhengyi Wang, Cheng Lu, Yikai Wang, Fan Bao, Chongxuan Li, Hang Su, and Jun Zhu. Prolificdreamer: High-fidelity and



- diverse text-to-3d generation with variational score distillation. *arXiv preprint arXiv:2305.16213*, 2023. 3
- [74] Daniel Watson, William Chan, Ricardo Martin-Brualla, Jonathan Ho, Andrea Tagliasacchi, and Mohammad Norouzi. Novel view synthesis with diffusion models. *arXiv preprint arXiv:2210.04628*, 2022. 3
- [75] Jamie Watson, Michael Firman, Gabriel J Brostow, and Daniyar Turmukhambetov. Self-supervised monocular depth hints. In *Proceedings of the IEEE/CVF international conference on computer vision*, pages 2162–2171, 2019. 2
- [76] Jinbo Wu, Xiaobo Gao, Xing Liu, Zhengyang Shen, Chen Zhao, Haocheng Feng, Jingtuo Liu, and Errui Ding. Hd-fusion: Detailed text-to-3d generation leveraging multiple noise estimation. *arXiv preprint arXiv:2307.16183*, 2023. 3
- [77] Jianfeng Xiang, Jiaolong Yang, Binbin Huang, and Xin Tong. 3d-aware image generation using 2d diffusion models. *arXiv preprint arXiv:2303.17905*, 2023. 3
- [78] Junyuan Xie, Ross Girshick, and Ali Farhadi. Deep3d: Fully automatic 2d-to-3d video conversion with deep convolutional neural networks. In *Computer Vision—ECCV 2016: 14th European Conference, Amsterdam, The Netherlands, October 11–14, 2016, Proceedings, Part IV 14*, pages 842–857. Springer, 2016. 6
- [79] Junyuan Xie, Ross Girshick, and Ali Farhadi. Deep3d: Fully automatic 2d-to-3d video conversion with deep convolutional neural networks. In *Computer Vision—ECCV 2016: 14th European Conference, Amsterdam, The Netherlands, October 11–14, 2016, Proceedings, Part IV 14*, pages 842–857. Springer, 2016. 2
- [80] Gangwei Xu, Xianqi Wang, Xiaohuan Ding, and Xin Yang. Iterative geometry encoding volume for stereo matching. In *Proc. IEEE Conf. Comp. Vis. Patt. Recogn.*, pages 21919–21928, 2023. 1, 6, 7, 8, 2
- [81] Haofei Xu and Juyong Zhang. Aanet: Adaptive aggregation network for efficient stereo matching. In *Proc. IEEE Conf. Comp. Vis. Patt. Recogn.*, pages 1959–1968, 2020. 5, 1, 2
- [82] Guorun Yang, Hengshuang Zhao, Jianping Shi, Zhidong Deng, and Jiaya Jia. Segstereo: Exploiting semantic information for disparity estimation. In *Proc. Eur. Conf. Comp. Vis.*, pages 636–651, 2018. 1, 2, 7
- [83] Guorun Yang, Xiao Song, Chaoqin Huang, Zhidong Deng, Jianping Shi, and Bolei Zhou. Drivingstereo: A large-scale dataset for stereo matching in autonomous driving scenarios. In *Proc. IEEE Conf. Comp. Vis. Patt. Recogn.*, pages 899–908, 2019. 1
- [84] Lihe Yang, Bingyi Kang, Zilong Huang, Xiaogang Xu, Jiashi Feng, and Hengshuang Zhao. Depth anything: Unleashing the power of large-scale unlabeled data. In *Proceedings of the IEEE/CVF Conference on Computer Vision and Pattern Recognition*, pages 10371–10381, 2024. 1
- [85] Lihe Yang, Bingyi Kang, Zilong Huang, Zhen Zhao, Xiaogang Xu, Jiashi Feng, and Hengshuang Zhao. Depth anything v2. *arXiv preprint arXiv:2406.09414*, 2024.
- [86] Wei Yin, Chi Zhang, Hao Chen, Zhipeng Cai, Gang Yu, Kaixuan Wang, Xiaozhi Chen, and Chunhua Shen. Metric3d: Towards zero-shot metric 3d prediction from a single image. In *Proceedings of the IEEE/CVF International Conference on Computer Vision*, pages 9043–9053, 2023. 1
- [87] Paul Yoo, Jiaxian Guo, Yutaka Matsuo, and Shixiang Shane Gu. Dreamspare: Escaping from plato’s cave with 2d frozen diffusion model given sparse views. *CoRR*, 2023. 3
- [88] Chaohui Yu, Qiang Zhou, Jingliang Li, Zhe Zhang, Zhibin Wang, and Fan Wang. Points-to-3d: Bridging the gap between sparse points and shape-controllable text-to-3d generation. *arXiv preprint arXiv:2307.13908*, 2023. 3
- [89] Jason J Yu, Adam W Harley, and Konstantinos G Derpanis. Back to basics: Unsupervised learning of optical flow via brightness constancy and motion smoothness. In *Computer Vision—ECCV 2016 Workshops: Amsterdam, The Netherlands, October 8–10 and 15–16, 2016, Proceedings, Part III 14*, pages 3–10. Springer, 2016. 1
- [90] Jason J. Yu, Fereshteh Forghani, Konstantinos G. Derpanis, and Marcus A. Brubaker. Long-term photometric consistent novel view synthesis with diffusion models. In *ICCV*, 2023. 3
- [91] F. Zhang, V. Prisacariu, R. Yang, and P. H. S. Torr. Ga-net: Guided aggregation net for end-to-end stereo matching. In *Proc. IEEE Conf. Comp. Vis. Patt. Recogn.*, 2019. 1
- [92] Lvmin Zhang, Anyi Rao, and Maneesh Agrawala. Adding conditional control to text-to-image diffusion models. In *Proceedings of the IEEE/CVF International Conference on Computer Vision*, pages 3836–3847, 2023. 3
- [93] Songyan Zhang, Zhicheng Wang, Qiang Wang, Jinshuo Zhang, Gang Wei, and Xiaowen Chu. Ednet: Efficient disparity estimation with cost volume combination and attention-based spatial residual. In *Proc. IEEE Conf. Comp. Vis. Patt. Recogn.*, pages 5429–5438, 2021. 1
- [94] Hang Zhao, Orazio Gallo, Iuri Frosio, and Jan Kautz. Loss functions for image restoration with neural networks. *IEEE Transactions on computational imaging*, 3(1):47–57, 2016. 5
- [95] Chao Zhou, Hong Zhang, Xiaoyong Shen, and Jiaya Jia. Unsupervised learning of stereo matching. In *Proc. IEEE Int. Conf. Comp. Vis.*, pages 1567–1575, 2017. 1, 2, 6, 7
- [96] Hang Zhou, David Greenwood, and Sarah Taylor. Self-supervised monocular depth estimation with internal feature fusion. *arXiv preprint arXiv:2110.09482*, 2021. 2, 8
- [97] Zhengming Zhou and Qiulei Dong. Self-distilled feature aggregation for self-supervised monocular depth estimation. In *European Conference on Computer Vision*, pages 709–726. Springer, 2022. 2, 8
- [98] Zhizhuo Zhou and Shubham Tulsiani. Sparsefusion: Distilling view-conditioned diffusion for 3d reconstruction. In *CVPR*, 2023. 3
- [99] Joseph Zhu and Peiye Zhuang. Hifa: High-fidelity text-to-3d with advanced diffusion guidance. *arXiv preprint arXiv:2305.18766*, 2023. 3